Available online at www.sciencedirect.com
ScienceDirect
Journal of Magnetic Resonance 191 (2008) 93–99
JMR Journal of Magnetic Resonance
www.elsevier.com/locate/jmr

Lorentz effect imaging of ionic currents in solution

Trong-Kha Truong *, Alexandru Avram, Allen W. Song

Brain Imaging and Analysis Center, Duke University Medical Center, P.O. Box 3918, Durham, NC 27710, USA

Received 30 August 2007; revised 28 November 2007
Available online 23 December 2007

Abstract

Current functional MRI techniques relying on hemodynamic modulations are inherently limited in their ability to accurately localize neural activity in space and time. To address these limitations, we previously proposed a novel technique based on the Lorentz effect and demonstrated its ability to directly image minute electrical activity with a millisecond temporal resolution in gel phantoms containing conductive wires as well as in the human median nerve *in vivo*. To better characterize its contrast mechanism and ultimately further improve its sensitivity for *in vivo* applications, we now apply this technique to image ionic currents in solution, which serve as a better model for neural conduction in biological systems than the electronic currents in conductive wires used in previous phantom studies. Our results demonstrate that ionic currents with durations and current densities on the same order of magnitude as those induced by neuroelectric activity in nerve fibers and in the brain can be detected.

Keywords: Lorentz effect imaging; Lorentz force; Ionic currents; Neuroelectric activity; Functional MRI

1. Introduction

Existing functional MRI (fMRI) techniques based on hemodynamic modulations, such as blood oxygenation level-dependent (BOLD) fMRI, are widely used to investigate the function of the human nervous system, but are inherently limited in their ability to accurately localize neural activity in space and time. As such, there has been an increasing interest over the past few years in the development of novel MRI techniques that can directly image neural activity *in vivo*, thereby combining the noninvasiveness and high spatial resolution advantages inherent in MRI with the high temporal resolution of modalities such as electroencephalography (EEG) and magnetoencephalography (MEG).

A number of studies have recently attempted to use MRI for detecting the minute magnetic field changes induced by neuronal currents [1]. These works included theoretical modeling [2–5] as well as experimental studies in phantoms [6–8], cell cultures [9], snail ganglia [10], optic nerves [11,12], and human brains, with both positive [13–17] and negative [18–20] findings. Despite some encouraging results, the direct imaging of neural activity *in vivo* has been challenging because of the extremely small activation-induced magnetic field changes as well as multiple synchronized confounding signals reflecting hemodynamic modulations or physiological noise.

To boost the signal detectability, we previously proposed an alternative technique called Lorentz effect imaging (LEI) [21] that can detect spatially incoherent yet temporally synchronized minute electrical activity in a strong magnetic field. We initially demonstrated its ability to directly image electrical currents on the order of microamperes with a temporal resolution on the order of milliseconds in gel phantoms containing conductive wires [22]. More recently, we successfully applied this technique to directly image neuroelectric activity *in vivo* in the human median nerve during electrical stimulation of the wrist [23]. Such a real-time and noninvasive neuroimaging technique may potentially find broad applications in neurosciences. To better characterize its contrast mechanism and

* Corresponding author. Fax: +1 919 681 7033.
E-mail address: truong@biac.duke.edu (T.-K. Truong).

1090-7807/$ - see front matter © 2007 Elsevier Inc. All rights reserved.
doi:10.1016/j.jmr.2007.12.005

gain new insights that could further improve its sensitivity for *in vivo* applications, we now apply the LEI technique to image ionic currents in solution, which are more relevant to neural conduction in biological systems and differ from the electronic currents in conductive wires used in previous phantom studies.

2. Methods

2.1. Theory

An ion with a charge q, a mass m, and a velocity $\mathbf{v}$ contained in an ionic solution exposed to an electric field $\mathbf{E}$ and a magnetic field $\mathbf{B}$ experiences a Lorentz force $\mathbf{F}_{\text{Lorentz}}$ and a drag force $\mathbf{F}_{\text{drag}}$ so that its equation of motion is given by:

$$\mathbf{F}_{\text{Lorentz}} + \mathbf{F}_{\text{drag}} = q(\mathbf{E} + \mathbf{v} \times \mathbf{B}) - b\mathbf{v} = m\,\mathrm{d}\mathbf{v}/\mathrm{d}t, \quad (1)$$

where b is a constant. In the case of a uniform static magnetic field $\mathbf{B}$ oriented along the z axis, Eq. (1) becomes:

$$q(E_x + v_y B) - bv_x = m\,\mathrm{d}v_x/\mathrm{d}t, \quad (2)$$

$$q(E_y - v_x B) - bv_y = m\,\mathrm{d}v_y/\mathrm{d}t. \quad (3)$$

Thus, in the presence of a spatially varying electric field, the ions contained in the solution, and consequently the water molecules surrounding them, experience a spatially incoherent displacement induced by the Lorentz force. In the LEI technique, a magnetic field gradient is applied so that the spins affected by such an incoherent displacement experience a dephasing proportional to its amplitude and duration, which in turn results in a signal loss within a voxel. Furthermore, multiple cycles of oscillating gradients synchronized with the Lorentz force (Fig. 1) can be applied to amplify the loss of phase coherence, and thus significantly increase the sensitivity of the technique [22,23].

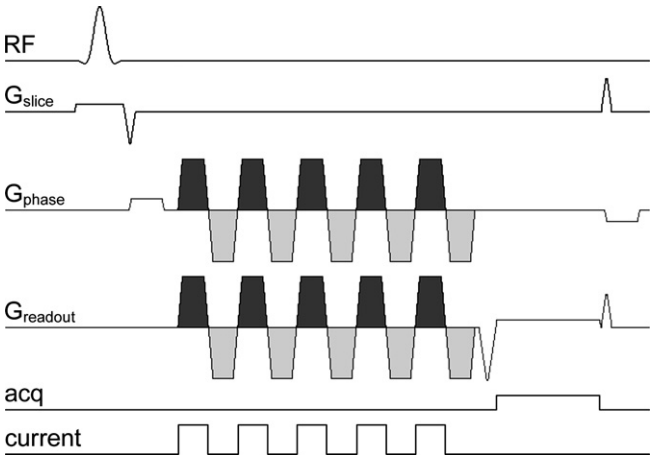

Fig. 1. Gradient echo pulse sequence diagram with multiple cycles of oscillating gradients applied in the readout and phase-encoding directions between excitation and data acquisition. The ionic current is synchronized with the pulse sequence such that it is turned on only during the positive lobes of the oscillating gradients.

2.2. Simulations

To get an insight into the trajectory of the ions experiencing the Lorentz effect, simulations were performed for the case of a sphere of diameter d containing a $CuSO_4$ solution and exposed to a dipolar electric field generated by two electrodes placed on each side of the sphere (Fig. 2). Assuming that these electrodes are located at $\mathbf{x}_1 = (-d/2; 0)$ and $\mathbf{x}_2 = (d/2; 0)$ with a voltage $U/2$ and $-U/2$, respectively, the electric field is given by:

$$\mathbf{E} = \frac{U}{2}\left[\frac{\mathbf{x} - \mathbf{x}_1}{|\mathbf{x} - \mathbf{x}_1|^2} - \frac{\mathbf{x} - \mathbf{x}_2}{|\mathbf{x} - \mathbf{x}_2|^2}\right]. \quad (4)$$

Eqs. (2) and (3) were numerically solved with an explicit Runge–Kutta algorithm for a series of Cu^{2+} and SO_4^{2-} ions initially at rest in the vicinity of the positive and negative electrodes, respectively, using the following parameters: $q(Cu^{2+}) = 3.204 \times 10^{-19}$ C, $q(SO_4^{2-}) = -3.204 \times 10^{-19}$ C, $m(Cu^{2+}) = 1.055 \times 10^{-25}$ kg, $m(SO_4^{2-}) = 1.595 \times 10^{-25}$ kg, $d = 10$ cm, $U = 5$ V, $B = 4$ T, and an empirically determined constant $b = 2.5 \times 10^{-18}$ kg/s. The simulations were performed in Maltab (The MathWorks, Inc., Natick, MA).

2.3. Experiments

To demonstrate the Lorentz effect in ionic solutions experimentally, a 10-cm diameter spherical phantom was filled with a 2.8 g/l $CuSO_4$ solution ($T_1 = 120$ ms, $T_2 = 75$ ms) and two copper wire electrodes were tightly inserted through holes located on each side of the phantom (Fig. 2). The electrodes had a diameter of 2 mm and a length of 4 mm inside the phantom, the electrical conduc-

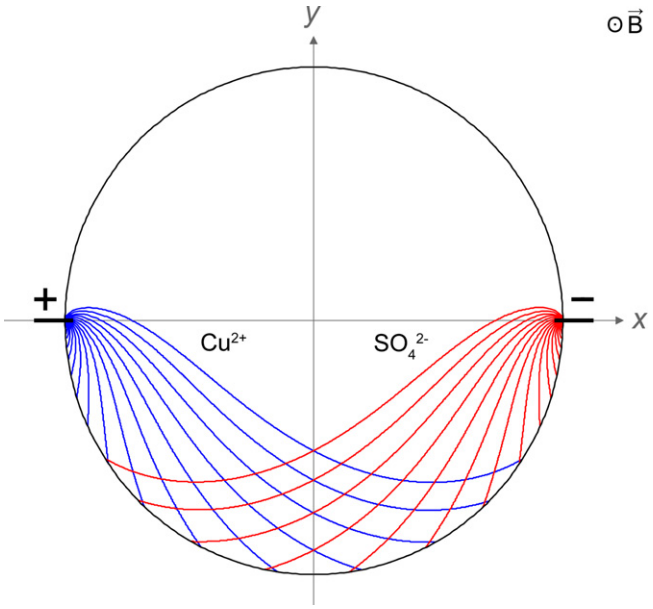

Fig. 2. Simulated trajectories of a series of Cu^{2+} and SO_4^{2-} ions in a sphere containing a $CuSO_4$ solution exposed to a uniform static magnetic field and a dipolar electric field induced by two electrodes located on each side of the sphere.

tivity of the solution was 1.4 S/cm, and the resistance of the phantom was 1 kΩ. The electrodes were positioned orthogonal to the main magnetic field and connected via shielded cables to a square wave pulse generator triggered by the scanner such that the current was turned on only during the positive lobes of the oscillating gradients. They were replaced regularly between experiments to prevent excessive electroplating.

Four experiments were performed at 20 °C on a 4 T MRI scanner (GE Healthcare, Milwaukee, WI) using a shielded quadrature birdcage head coil and whole-volume high-order shimming. Gradient echo images were acquired using the following parameters: repetition time (TR) 150 ms, echo time (TE) 71 ms, flip angle 60°, field-of-view 12 cm, matrix size 256×128, and slice thickness 5 mm.

Experiments 1 and 2 were performed to investigate the signal dependence on the current amplitude, the current polarity, and the oscillating gradients, and thus validate the contrast mechanism of the LEI technique for ionic currents in solution. In Experiment 1, an axial slice containing both electrodes was successively acquired using a current amplitude of 0, 0.1, 0.2, 0.5, 1, 2, and 5 mA, with both positive and negative polarity. Four averages were used for current amplitudes below 0.5 mA to increase the signal-to-noise ratio. A total of 15 cycles of oscillating gradients with an amplitude of 36 mT/m and a duration of 2 ms for each lobe were applied along both the readout and phase-encoding directions. The resulting *b*-factor was only 9 s/mm^2, thus causing negligible signal attenuation due to diffusion weighting. In Experiment 2, the same axial slice was acquired using a current of 0 and 5 mA, but with no oscillating gradients applied.

The current pulse duration in the previous experiments was 2 ms, which is on the same order of magnitude as neuroelectric activity induced in nerve fibers. To demonstrate that the LEI technique can also detect ionic currents similar to those induced by neural activity in the brain, which last on the order of tens of milliseconds, Experiment 3 was performed using a longer current pulse duration of 10 ms and oscillating gradient parameters adjusted accordingly. A total of three cycles of oscillating gradients with an amplitude of 9 mT/m and a duration of 10 ms for each lobe were applied to maintain the same *b*-factor and imaging parameters as in Experiment 1, and the same axial slice was acquired using a current of 0 and 5 mA.

Finally, Experiment 4 was performed to better assess the spatial characteristics of the signal changes over a three-dimensional volume and to estimate the ionic current density that can be detected. A series of 19 contiguous slices covering the whole phantom were acquired with a current of 0 and 5 mA using the same oscillating gradients as in Experiment 1. A sagittal slice orientation was chosen to provide a high spatial resolution in both directions orthogonal to the direction of the ionic current, and thus allow a more accurate estimation of the current density. The different slices were acquired separately rather than using a multislice acquisition to ensure that only one train of current pulses was triggered per TR period.

3. Results

3.1. Simulations

The results of the simulations (Fig. 2) show that the Cu^{2+} and SO_4^{2-} ions, although moving in opposite directions towards the negative and positive electrode respectively, both follow trajectories that are curved downwards, as predicted by the direction of the Lorentz force (see Eq. (1)). As such, their envelope forms a characteristic ''banana-shaped'' trajectory between both electrodes. Although these simulations did not take into account effects such as the boundary conditions or interactions between ions, they do nevertheless provide an insight into the overall trajectory of the ionic current, which can be compared with the experimental results.

3.2. Experiment 1: signal dependence on the ionic current amplitude and polarity

The results of Experiment 1 are shown in Fig. 3. The images acquired with different ionic currents (Fig. 3a) show a predominant signal loss along a curved trajectory between both electrodes, consistent with the simulations. This effect gradually increases with the current amplitude, which can be better visualized on the difference images obtained by subtracting the reference image acquired without current from each image (Fig. 3b). Furthermore, the trajectory is curved downwards or upwards for positive and negative currents respectively, as predicted by the direction of the Lorentz force. Although signal loss is predominant, there are also some regions with signal increase due to flow effects, which will be discussed in Section 4.

3.3. Experiment 2: signal dependence on the oscillating gradients

The results of Experiment 2 (Fig. 4), in which images were acquired with a current but without oscillating gradients, show no significant signal changes, demonstrating that oscillating gradients synchronized with the current are critical to generate a contrast. This control experiment thus confirms that the dominant contrast mechanism in Experiment 1 is indeed the loss of phase coherence generated by the oscillating gradients of the spins experiencing a spatially incoherent displacement due to the Lorentz force. Furthermore, these results also demonstrate that there is no signal loss caused by susceptibility effects of micro-bubbles formed during electrolysis or by the magnetic field induced by the ionic current. The characteristic signal dependence on the current amplitude, the current polarity, and the oscillating gradients, observed in Experiments 1 and 2, and previously demonstrated for electronic currents in conductive wires [22], thus validates the basic

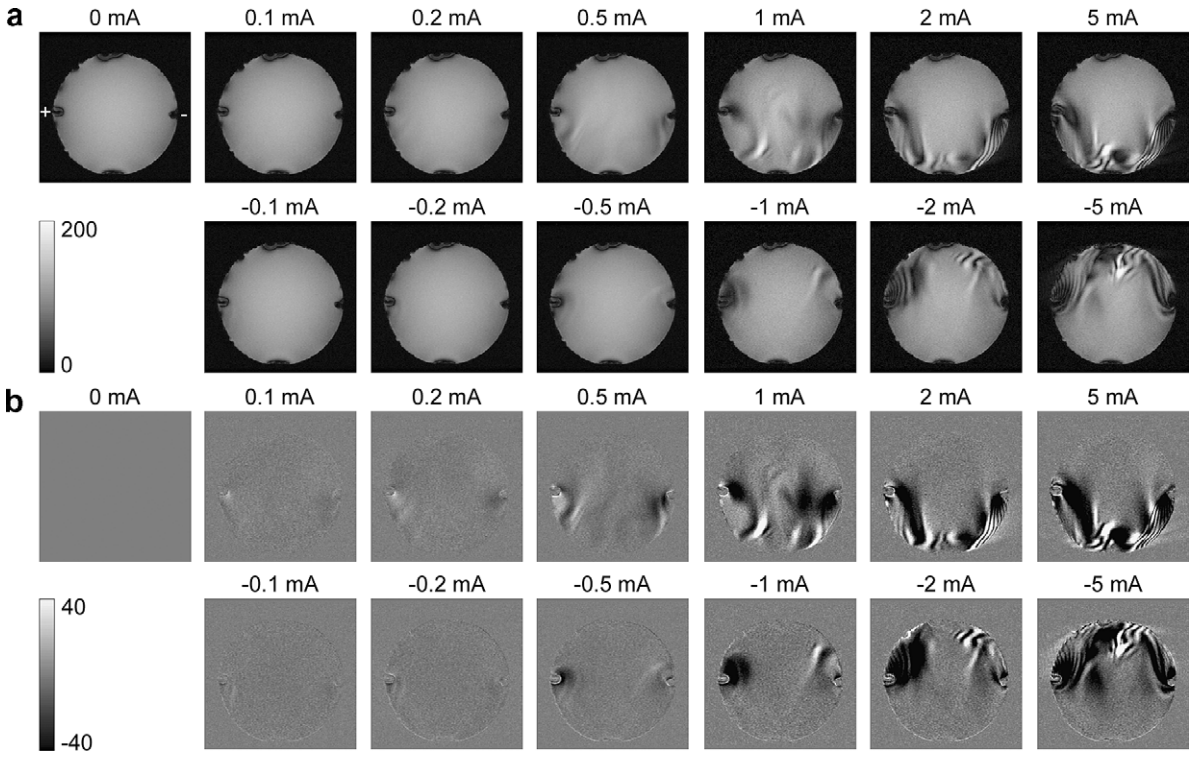

Fig. 3. Experiment 1. (a) Axial images of the phantom acquired with different ionic current amplitudes and polarities using 15 cycles of oscillating gradients with a duration of 2 ms for each lobe. (b) Difference images obtained by subtracting the reference image acquired without current from each image in (a). The main magnetic field points out of the image plane. The signal intensity in (a) and (b) is expressed as a percentage of the mean signal intensity inside the phantom in the image acquired without current.

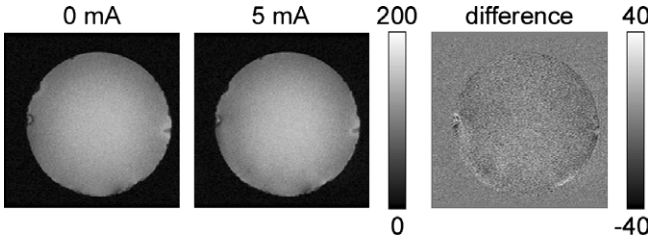

Fig. 4. Experiment 2. Axial images of the phantom acquired without and with current but no oscillating gradients, and resulting difference image. The signal intensity is expressed as a percentage of the mean signal intensity inside the phantom in the image acquired without current.

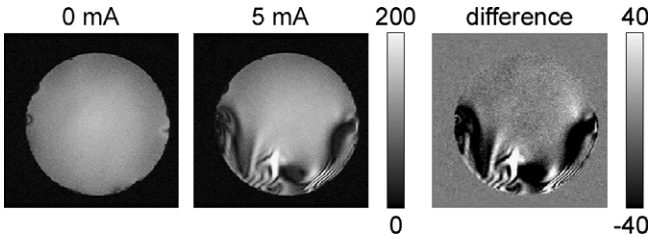

Fig. 5. Experiment 3. Axial images of the phantom acquired without and with current using three cycles of oscillating gradients with a duration of 10 ms for each lobe, and resulting difference image. The signal intensity is expressed as a percentage of the mean signal intensity inside the phantom in the image acquired without current.

contrast mechanism of the LEI technique for ionic currents in solution.

3.4. Experiment 3: signal dependence on the ionic current duration

The results of Experiment 3 (Fig. 5), in which a longer current pulse duration was used, are very similar to those obtained in Experiment 1 with a current of 5 mA. These experiments thus demonstrate that the LEI technique can detect ionic currents with a duration ranging from milliseconds to tens of milliseconds, which is on the same order of magnitude as neuroelectric activity induced in nerve fibers and in the brain, respectively.

3.5. Experiment 4: signal dependence over a three-dimensional volume

The results of Experiment 4 are shown in Fig. 6. The images acquired without current were first subtracted from those acquired with a 5 mA current. To better visualize the spatial characteristics of the signal changes over the whole phantom, ''activated'' voxels were defined as those experiencing an absolute signal change exceeding a given threshold, ranging from 20% to 60% of the mean signal intensity inside the phantom in the images acquired without current. These voxels were defined using both positive and negative signal changes in order to obtain a continuous trajectory for the ionic current. The resulting volumes of activated

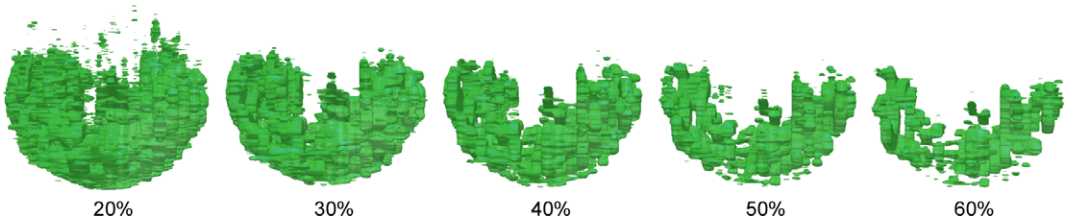

Fig. 6. Experiment 4. Volumes of "activated" voxels, defined as those experiencing an absolute signal change exceeding the threshold indicated below each image, expressed as a percentage of the mean signal intensity inside the phantom in the images acquired without current.

voxels (Fig. 6) clearly show a three-dimensional "banana-shaped" trajectory between both electrodes in the lower hemisphere of the phantom, consistent with the simulations and the results of Experiments 1 and 3. Lower thresholds result in a larger number of isolated clusters of activated voxels outside of the main volume, whereas higher thresholds result in a larger number of holes inside. However, the overall shape of the trajectory is preserved across the range of thresholds. The optimal threshold for which the activated volume best covers the full trajectory of the ionic current was determined to be 40%.

4. Discussion

4.1. Flow effects

Our experiments have shown that the LEI technique can be applied to image ionic currents in solution and that its dominant contrast mechanism is the signal loss caused by the intravoxel incoherent displacement of the spins experiencing the Lorentz effect. However, there are also some regions with cyclic alternations of signal increase and decrease along the trajectory of the ionic current. These signal changes are due to the bulk motion of water molecules induced by the displacement of the ions, as in-plane motion of spins in the presence of magnetic field gradients causes phase shifts that can lead to constructive or destructive interference, resulting in a signal increase or decrease in magnitude images. Flow effects can thus help enhance the contrast in the presence of oscillating gradients. However, the displacement of water molecules induced by the ions can potentially extend over distances larger than the voxel size, thereby reducing the spatial specificity of the activation maps. Nevertheless, our simulations have shown that the overall trajectory of the ionic current (Fig. 2) is generally in good agreement with the volume of activated voxels (Fig. 6), indicating that the spatial dispersion is not very significant. Furthermore, a histogram of the signal difference inside the phantom between the images acquired with and without current in Experiment 4 (Fig. 7) shows that the proportion of activated voxels experiencing a signal decrease is significantly larger than the proportion of activated voxels experiencing a signal increase, confirming that flow effects only have a small contribution to the overall signal changes. More importantly, while such effects are clearly visible in our experiments because flow was not restricted inside the phantom, they are expected to be significantly smaller for *in vivo* applications, since the movement of water molecules in biological tissues is restricted over distances much shorter than the voxel size.

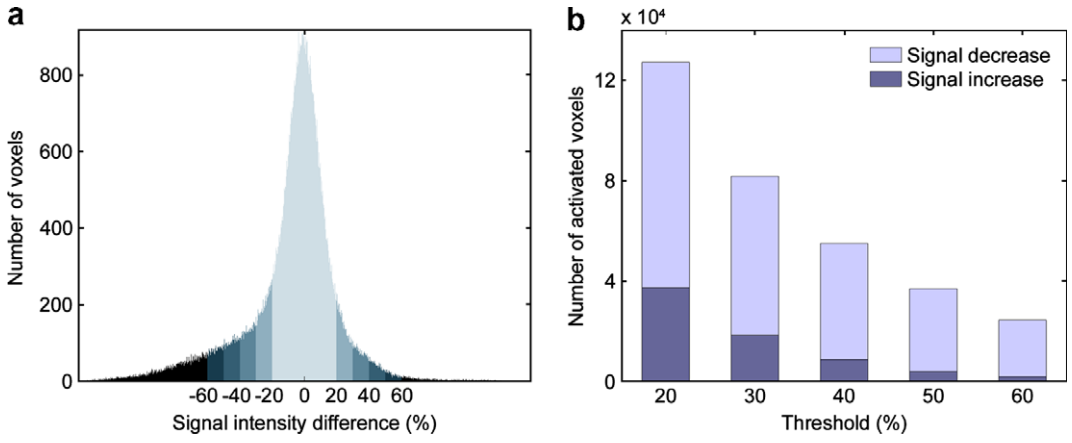

Fig. 7. Experiment 4. (a) Histogram of the signal intensity difference inside the phantom between the images acquired with and without current. (b) Number of activated voxels experiencing a signal decrease or a signal increase for different thresholds. The signal intensity in (a) and the thresholds in (b) are expressed as a percentage of the mean signal intensity inside the phantom in the images acquired without current.

4.2. Estimation of the current density

The volume of activated voxels from Experiment 4 (defined using the optimal threshold of 40%) was used to estimate the ionic current density. To this end, the total current amplitude (5 mA) was divided by the cross-sectional area of the volume for each sagittal slice. This calculation assumes that the ionic current is orthogonal to each cross-section, which is not true in the vicinity of the electrodes where the trajectory is significantly curved. Furthermore, the current density can be expected to be higher near the electrodes and lower at the center of the phantom. As such, only the five central sagittal slices were used, and the average ionic current density was found to be 7.5 μA/mm^2. Since some of the activated voxels, which were defined using both positive and negative signal changes, could potentially be attributed entirely to flow effects, the current density might be underestimated. Nevertheless, this value is on the same order of magnitude as the current densities previously detected with the LEI technique in gel phantoms containing conductive wires [22] and, more importantly, as those generated by the synchronized activity of a functional cortical unit in the brain, typically consisting of 10^4–10^5 neurons/mm^2 [24]. In Experiment 4, a relatively high current amplitude was used to induce large signal changes along the full trajectory between both electrodes, and thus allow a more accurate estimation of its cross-sectional area for each slice. However, as shown in Experiment 1, significant signal changes can still be detected at lower current amplitudes. Furthermore, the sensitivity of the LEI technique can be independently increased by using a larger number of averages, a higher magnetic field strength, and/or stronger oscillating gradients. These results thus support its potential application to biological systems.

5. Conclusions

Our studies have demonstrated that the LEI technique can be applied to image ionic currents in solution. The characteristic signal dependence on the current amplitude, the current polarity, and the oscillating gradients was observed, thus validating its basic contrast mechanism. Ionic currents with durations and current densities on the same order of magnitude as those induced by neuroelectric activity in nerve fibers and in the brain were detected, confirming its adequate sensitivity. Further studies are currently underway to apply and optimize this technique for *in vivo* applications.

Acknowledgment

This work was supported by Grant BES 0602529 from the National Science Foundation.

References

[1] P.A. Bandettini, N. Petridou, J. Bodurka, Direct detection of neuronal activity with MRI: fantasy, possibility, or reality? Appl. Magn. Reson. 29 (2005) 65–88.
[2] Y. Xue, J.-H. Gao, J. Xiong, Direct MRI detection of neuronal magnetic fields in the brain: theoretical modeling, NeuroImage 31 (2006) 550–559.
[3] T.S. Park, S.Y. Lee, Effects of neuronal magnetic fields on MRI: numerical analysis with axon and dendrite models, NeuroImage 35 (2007) 531–538.
[4] Q. Luo, H.-L. Liu, B. Parris, H. Lu, D.M. Senseman, J.-H. Gao, Modeling oxygen effects in tissue-preparation neuronal-current MRI, Magn. Reson. Med. 58 (2007) 407–412.
[5] K.B. Blagoev, B. Mihaila, B.J. Travis, L.B. Alexandrov, A.R. Bishop, D. Ranken, S. Posse, C. Gasparovic, A. Mayer, C.J. Aine, I. Ulbert, M. Morita, W. Müller, J. Connor, E. Halgrenm, Modelling the magnetic signature of neuronal tissue, NeuroImage 37 (2007) 137–148.
[6] J. Bodurka, A. Jesmanowicz, J.S. Hyde, H. Xu, L. Estkowski, S.J. Li, Current-induced magnetic resonance phase imaging, J. Magn. Reson. 137 (1999) 265–271.
[7] J. Bodurka, P.A. Bandettini, Toward direct mapping of neuronal activity: MRI detection of ultraweak, transient magnetic fields changes, Magn. Reson. Med. 47 (2002) 1052–1058.
[8] D. Konn, P. Gowland, R. Bowtell, MRI detection of weak magnetic fields due to an extended current dipole in a conducting sphere: a model for direct detection of neuronal currents in the brain, Magn. Reson. Med. 50 (2003) 40–49.
[9] N. Petridou, D. Plenz, A.C. Silva, M. Loew, J. Bodurka, P.A. Bandettini, Direct magnetic resonance detection of neuronal electrical activity, Proc. Natl. Acad. Sci. USA 103 (2006) 16015–16020.
[10] T.S. Park, S.Y. Lee, J.-H. Park, M.H. Cho, S.Y. Lee, Observation of the fast response of a magnetic resonance signal to neuronal activity: a snail ganglia study, Physiol. Meas. 27 (2006) 181–190.
[11] L.S. Chow, G.G. Cook, E. Whitby, M.N.J. Paley, Investigating direct detection of axon firing in the adult human optic nerve using MRI, NeuroImage 30 (2006) 835–846.
[12] L.S. Chow, G.G. Cook, E. Whitby, M.N.J. Paley, Investigation of MR signal modulation due to magnetic fields from neuronal currents in the adult human optic nerve and visual cortex, Magn. Reson. Imaging 24 (2006) 681–691.
[13] H. Kamei, K. Iramina, K. Yoshikawa, S. Ueno, Neuronal current distribution imaging using magnetic resonance, IEEE Trans. Magn. 35 (1999) 4109–4111.
[14] J. Xiong, P.T. Fox, J.H. Gao, Directly mapping magnetic field effects of neuronal activity by magnetic resonance imaging, Hum. Brain Mapp. 20 (2003).
[15] M. Bianciardi, F. Di Russo, T. Aprile, B. Maraviglia, G.E. Hagberg, Combination of BOLD-fMRI and VEP recordings for spin-echo MRI detection of primary magnetic effects caused by neuronal currents, Magn. Reson. Imaging 22 (2004) 1429–1440.
[16] D. Konn, S. Leach, P. Gowland, R. Bowtell, Initial attempts at directly detecting alpha wave activity in the brain using MRI, Magn. Reson. Imaging 22 (2004) 1413–1427.
[17] L.S. Chow, G.G. Cook, E. Whitby, M.N.J. Paley, Investigation of axonal magnetic fields in the human corpus callosum using visual stimulation based on MR signal modulation, J. Magn. Reson. Imaging 26 (2007) 265–273.
[18] R. Chu, J.A. de Zwart, P. van Gelderen, M. Fukunaga, P. Kellman, T. Holroyd, J.H. Duyn, Hunting for neuronal currents: absence of rapid MRI signal changes during visual-evoked response, NeuroImage 23 (2004) 1059–1067.
[19] L.M. Parkes, F.P. de Lange, P. Fries, I. Toni, D.G. Norris, Inability to directly detect magnetic field changes associated with neuronal activity, Magn. Reson. Med. 57 (2007) 411–416.
[20] H. Mandelkow, P. Halder, D. Brandeis, M. Soellinger, N. de Zanche, R. Luechinger, P. Boesiger, Heart beats brain: the problem of

detecting alpha waves by neuronal current imaging in joint EEG–MRI experiments, NeuroImage 37 (2007) 149–163.
[21] A.W. Song, A.M. Takahashi, Lorentz effect imaging, Magn. Reson. Imaging 19 (2001) 763–767.
[22] T.-K. Truong, J.L. Wilbur, A.W. Song, Synchronized detection of minute electrical currents with MRI using Lorentz effect imaging, J. Magn. Reson. 179 (2006) 85–91.
[23] T.-K. Truong, A.W. Song, Finding neuroelectric activity under magnetic-field oscillations (NAMO) with magnetic resonance imaging *in vivo*, Proc. Natl. Acad. Sci. USA 103 (2006) 12598–12601.
[24] M. Hämäläinen, R. Hari, R.J. Ilmoniemi, J. Knuutila, O.V. Lounasmaa, Magnetoencephalography—theory, instrumentation, and applications to noninvasive studies of the working human brain, Rev. Mod. Phys. 65 (1993) 413–497.